Geophysical Research Letters

RESEARCH LETTER
10.1029/2025GL118727

Crustal Flow-Driven Plateau Growth and Expansion Front in NE Tibet: Insights From High-Resolution Attenuation Tomography With High-Density ChinArray Lg Data

Ruo-Jie Li[1,2], Lian-Feng Zhao[1,3], Xiao-Bi Xie[4], Xi He[1], and Zhen-Xing Yao[1]

[1]Key Laboratory of Planetary Science and Frontier Technology, Institute of Geology and Geophysics, Chinese Academy of Sciences, Beijing, China, [2]College of Earth and Planetary Sciences, University of Chinese Academy of Sciences, Beijing, China, [3]Heilongjiang Mohe Observatory of Geophysics, Institute of Geology and Geophysics, Chinese Academy of Sciences, Beijing, China, [4]Institute of Geophysics and Planetary Physics, University of California, Santa Cruz, CA, USA

Abstract The Northeastern (NE) Tibet, as the front of plateau growth, widely absorbs northeastward extrusion, leading to significant uplift and forming a basin-mountain tectonic framework. However, it remains unclear how the crust of NE Tibet deformed in response to the far-field effects of the India-Eurasia collision. Here, we construct a high-resolution broadband crustal Q_{Lg} model in NE Tibet using seismic attenuation tomography based on high-density ChinArray Lg data. Strong Lg attenuation was observed beneath the Songpan-Ganzi, suggesting crustal ductile material flow. The Qilian orogeny, characterized by relatively weak low-Q_{Lg} anomalies, may have experienced an early stage of plateau formation. The lateral variation in crustal rheology, as revealed by the Lg attenuation gradient, exhibits a distinct strength contrast between the plateau interior and the forelands, indicating a crustal-scale boundary of plateau expansion. Cenozoic tectonic extrusion and subsequent ductile material flow jointly govern the crustal deformation of NE Tibet.

Plain Language Summary Dense permanent and multi-stage mobile networks, including the ChinArray-Himalaya II, recorded a large amount of high-quality data, providing an unprecedented opportunity to investigate the crustal attenuation structure beneath northeastern (NE) Tibet. We construct a high-resolution broadband Lg-wave attenuation model for this region to constrain crustal rheology, calculate the Q_{Lg} gradient, and use its steepest segment to distinguish the soft, hot, ductile plateau from the hard, cold, rigid cratonic basins at the crustal scale. From this, we determined the boundary of plateau expansion and gained a better understanding of crustal deformation mechanisms in NE Tibet. The Q_{Lg} model between 0.3 and 2.0 Hz provides the best characterization for regional geological blocks. Pronounced low-Q_{Lg} anomalies, widely distributed in the Songpan-Ganzi and West Qinling, are inferred to result from crustal ductile material flow on a geological timescale. To the north, in contrast, the isolated low-Q_{Lg} zone beneath the Qilian orogen possibly originates from brittle crustal shortening. Our results support the coexistence of ductile crustal flow and brittle deformation, thereby enhancing understanding of tectonic evolution in NE Tibet.

Key Points:

- A high-resolution broadband crustal Lg-wave attenuation structure is established in Northeastern (NE) Tibet
- Strong Lg attenuation indicates potential ductile crustal flow beneath the Songpan-Ganzi block and possible brittle Qilianshan shortening
- Multiple crustal deformation mechanisms may jointly control the tectonic evolution of the NE margin of the Tibetan Plateau

Supporting Information:

Supporting Information may be found in the online version of this article.

Correspondence to:

L.-F. Zhao,
zhaolf@mail.iggcas.ac.cn

Citation:

Li, R.-J., Zhao, L.-F., Xie, X.-B., He, X., & Yao, Z.-X. (2026). Crustal flow-driven plateau growth and expansion front in NE Tibet: Insights from high-resolution attenuation tomography with high-density ChinArray Lg data. *Geophysical Research Letters*, *53*, e2025GL118727. https://doi.org/10.1029/2025GL118727

Received 11 AUG 2025
Accepted 9 JAN 2026

Author Contributions:

Conceptualization: Ruo-Jie Li, Lian-Feng Zhao, Xiao-Bi Xie, Xi He
Data curation: Lian-Feng Zhao
Formal analysis: Ruo-Jie Li, Lian-Feng Zhao, Xi He
Funding acquisition: Lian-Feng Zhao, Zhen-Xing Yao
Investigation: Ruo-Jie Li
Methodology: Ruo-Jie Li, Lian-Feng Zhao, Xiao-Bi Xie, Xi He, Zhen-Xing Yao
Project administration: Lian-Feng Zhao, Zhen-Xing Yao
Software: Ruo-Jie Li, Lian-Feng Zhao, Xi He
Supervision: Lian-Feng Zhao, Xiao-Bi Xie, Zhen-Xing Yao

1. Introduction

The Cenozoic India-Eurasia collision uplifted the northeastern Tibetan Plateau (NETP), forming high topography and notable crustal thickening at the plateau expansion front (Figure 1) (e.g., Molnar & Tapponnier, 1975). GPS measurements show substantial northeastward surface motion in northeastern (NE) Tibet (e.g., Y. H. Li et al., 2018), whereas the upper and lower crustal deformations are inferred to be mechanically decoupled (Karplus et al., 2013; S. Y. Zhang et al., 2022). Consequently, how deep crustal deformation responds to the far-field effects of India-Eurasia convergence and the mechanisms of plateau growth in NE Tibet remain debated. The controversy centers on two end-member dynamic models: brittle crustal shortening (Hubbard & Shaw, 2009) and ductile middle-to-lower crustal flow (Clark & Royden, 2000; Royden et al., 1997). The former is supported by the crustal wedge structure between the NETP and the North China Craton (NCC) revealed by receiver function imaging (Tian et al., 2021; Ye et al., 2015). For the latter, numerous geophysical investigations reveal that the crust in the NETP is characterized by low wave velocity, strong attenuation, high conductivity, and significant anisotropy, thus supporting the crustal flow model (Hao et al., 2021; X. B. Wang et al., 2014; L. F. Zhao et al., 2013; P. P. Zhao et al., 2021). Which of the abovementioned models dominates crustal deformation in NE Tibet, or if both operate, remains poorly understood. Consequently, whether the crustal ductile flow extrudes

Validation: Ruo-Jie Li, Lian-Feng Zhao, Xi He
Visualization: Ruo-Jie Li, Xi He
Writing – original draft: Ruo-Jie Li
Writing – review & editing: Ruo-Jie Li, Lian-Feng Zhao, Xiao-Bi Xie, Xi He

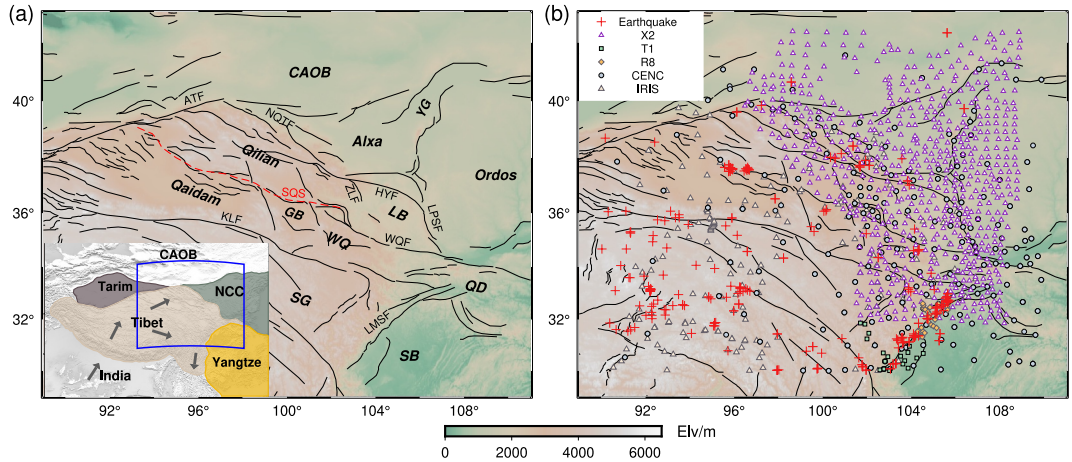

Figure 1. (a) Topographic map showing the tectonic units, main faults (black lines), and sutures (red dashed lines) in Northeastern Tibet and its adjacent areas. The inset illustrates the tectonic framework of East Asia, the study region's location (blue box), and the movement directions of the Indian Plate and Tibetan Plateau (dark gray arrows, from M. Wang & Shen, 2020). The abbreviations for tectonic units are as follows: CAOB, Central Asian Orogenic Belt; GB, Gonghe Basin; LB, Longxi Basin; NCC, North China Craton; QD, Qinling-Dabie Orogen; SB, Sichuan Basin; SG, Songpan-Ganzi terrane; WQ, West Qinling orogen; YG, Yinchuan graben. The faults and sutures are as follows: ATF, Altyn Tagh fault; HYF, Haiyuan fault; KLF, Kunlun fault; LMSF, Longmenshan fault; LPSF, Liupanshan fault; NQTF, North Qilian thrust faults; SQS, South Qilian suture; WQF, West Qinling fault; ZLF, Zhuanglanghe fault. (b) Locations of seismic stations and events (red crosses) in this region. The stations were from ChinArray-Himalaya II (X2), a Broadband mobile seismic array (T1), a Temporary observation array after the Wenchuan earthquake (M8.0) of 12 May 2008 (R8), the China Earthquake Networks Center, and the Incorporated Research Institutions for Seismology.

through its NE branches, as predicted in numerical modeling (Royden et al., 1997), and whether such extrusion controls the plateau expansion boundary (Hao et al., 2021; S. Li et al., 2022) remain hotly debated.

Seismic attenuation is sensitive to certain status and properties of crustal materials, for example, mineral composition, fractures, fluid content, temperature, and partial melting (Amalokwu et al., 2014; Karato & Spetzler, 1990; Kong et al., 2013; Winkler & Nur, 1982). Using Lg-wave attenuation data, previous studies successfully constrained the rheological and thermal anomalies in the crust (e.g., X. Y. Bao et al., 2011; X. He et al., 2021; L. F. Zhao et al., 2013). To better understand the mechanisms of plateau expansion and potential crustal material escape, high-density ChinArray-Himalaya II Lg-wave data are used to construct a high-resolution broadband crustal attenuation model in NE Tibet. The resulting crustal attenuation structure delineates the plateau expansion front at the crustal scale, providing new constraints for the dynamic mechanism of plateau growth in NE Tibet.

2. Data and Methods

Our data set comprises 26,019 vertical-component digital Lg waveforms recorded at 1,256 stations from 196 earthquakes between January 2000 and September 2018, with their ray paths crossing the NE Tibet and adjacent regions (Figure 1b, Table S1 in Supporting Information S1). Only crustal earthquakes with m_b 4.0–6.5 and distances of 200–2,000 km were selected to avoid impacts from complex rupture processes of large earthquakes (Figure S1, Table S2 in Supporting Information S1). The focal depths were shallower than the Moho discontinuity from CRUST1.0 (Laske et al., 2013).

By scanning waveforms with a 2.8–3.7 km/s sampling window, the Lg signal was identified using a 0.6 km/s-long group velocity window for maximum energy (X. He et al., 2021; L. F. Zhao et al., 2010). Waveform energy maxima generally fell within the 3.0–3.6 km/s group velocity window. Pre-P and pre-Lg noise series were then sampled using an equal-length time window (Figure S2 in Supporting Information S1) (e.g., Xie & Mitchell, 1990). The Lg and noise spectra were calculated at 58 discrete frequencies, log-evenly distributed between 0.05 and 10 Hz. A signal-to-noise ratio threshold of 2.0 for pre-Pn noise and 1.0 for pre-Lg noise was used for data quality control (L. F. Zhao et al., 2013). A joint tomography inversion method, utilizing single- and two-station Lg spectra, was used to construct a crustal attenuation model in NE Tibet (Text S1 in

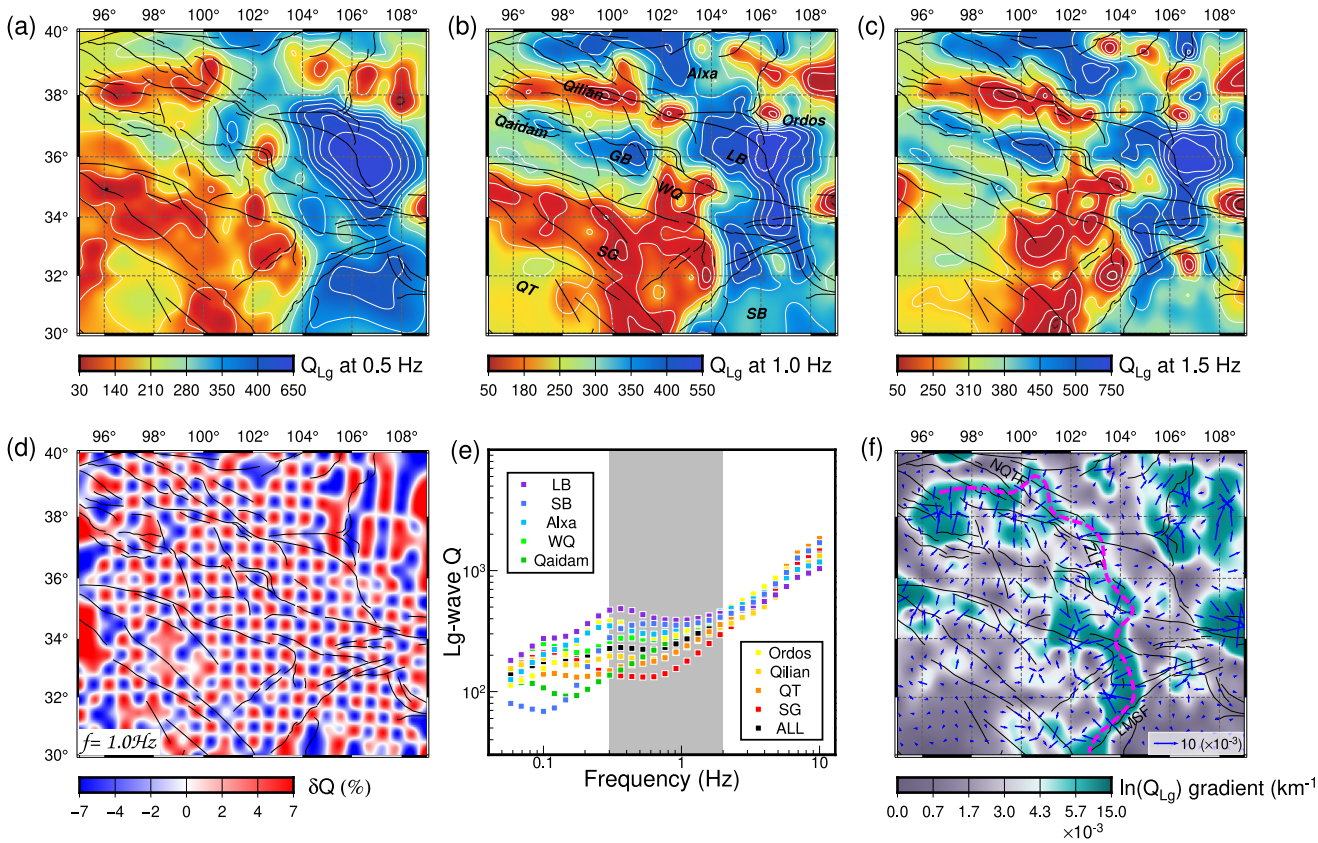

Figure 2. (a)–(c) Selected Q_{Lg} maps at 0.5, 1.0, and 1.5 Hz; note that different color scales are used. Black lines denote the main faults. (d) 0.5° × 0.5° checkerboard test at 1.0 Hz. (e) Mean Q_{Lg} versus frequency for different geo-blocks, with their values listed in Table S3 in Supporting Information S1. The block names are labeled in both panels (b) and (e). QT: Qiangtang terrane. Other abbreviations as in Figure 1a. (f) Crustal Q_{Lg}-gradient map. Gray and green denote low- and high-gradient areas, respectively. Blue arrows indicate the directions and magnitudes of the Q_{Lg} gradients, pointing toward the direction of Q decrease. The magenta dashed line denotes the defined high Q_{Lg}-gradient boundary.

Supporting Information S1, e.g., L. F. Zhao et al., 2013). A least squares orthogonal factorization algorithm (Paige & Sanders, 1982) was employed to simultaneously invert for source excitation and Q values at individual frequencies. A 0.5° grid was used for inversion, selected through grid-size tests to balance solution robustness and sensitivity (Figure S3 in Supporting Information S1). Grid neighborhood averaging was adopted. After inversion, the mean and standard deviation of the data residuals were significantly reduced at all frequencies, with error distributions becoming sharper and more unbiased (Figure S4 in Supporting Information S1). The site responses of all stations can be further inverted from the unresolved data residuals (Figure S5 in Supporting Information S1). Checkerboard tests with a 0.5° × 0.5° grid were conducted for resolution analysis of Q_{Lg} tomography at each frequency, constructed by adding ±7% logarithmic attenuation perturbations to a background Q (L. F. Zhao et al., 2013). Due to high-density ray coverage, the lateral resolution can reach 0.5° or higher in well-covered areas (Figure 2d and Figure S6 in Supporting Information S1). High stability is obtained across most of the imaging domain by estimating the Q uncertainty using the bootstrap method (Efron, 1979) (Figure S7 in Supporting Information S1).

3. Results

A broadband Lg-wave crustal attenuation model with unprecedented resolution for NE Tibet was developed, comprising Q_{Lg} distributions at 58 frequencies spanning 0.05–10 Hz. Although Q_{Lg} maps at different frequencies are not identical, they show consistent large-scale patterns. There are two prominent low-Q_{Lg} zones in NE Tibet (Figures 2a–2c). Analyzing the resulting Q values at individual frequencies indicates that the Q_{Lg} values of geo-blocks generally increase with frequency (Figures 2e and Figure S8 in Supporting Information S1). Given the fluctuation of single-frequency Q_{Lg}, a broadband Q_{Lg}, obtained by averaging log Q_{Lg} between 0.3 and 2.0 Hz

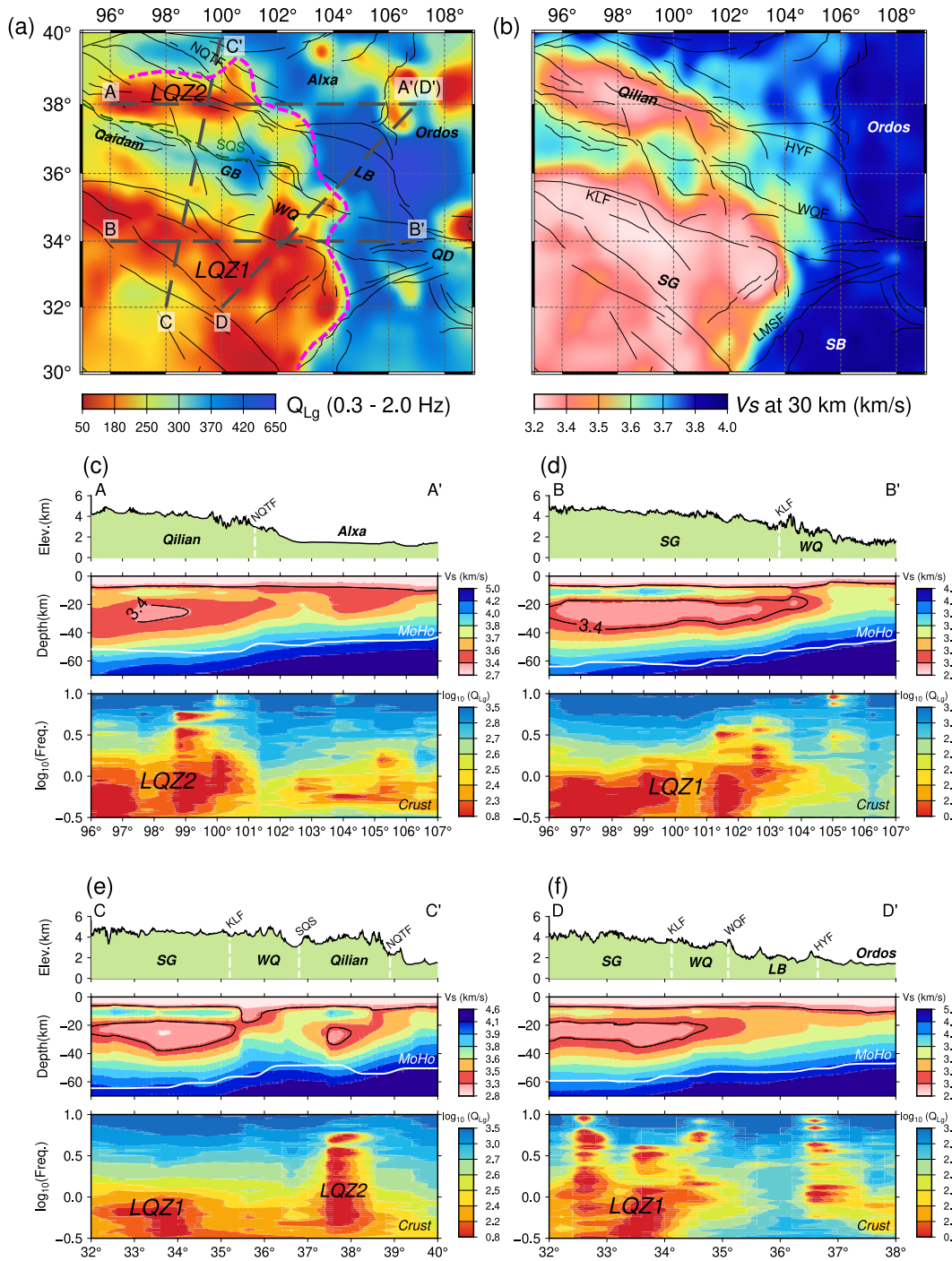

Figure 3. Comparison among the attenuation, shear wave velocity, and other integrated cross-sections in Northeastern Tibet. (a) Broadband crustal Q_{Lg} (0.3–2.0 Hz) map (this study); (b) S-wave velocities at 30 km depth (from Han et al., 2022). (c)–(f) Cross-sections A-A′, B-B′, C-C′, and D-D′ showing surface topography (upper), *Vs* versus depth (Han et al., 2022) (middle), and Q_{Lg} versus frequency (bottom). Surface locations of cross-sections are marked in (a) with gray dashed lines. The contours of *Vs* = 3.4 km/s are also marked in (c) and (d). Abbreviations as in Figure 1a. Moho discontinuities in *Vs* profiles are from the CRUST1.0 model (Laske et al., 2013). The magenta dashed line in (a) marks the sharp Q_{Lg} variation determined by the gradient.

(e.g., X. He et al., 2021), is chosen to characterize the crustal Lg attenuation (Figure 3a). By fitting the power-law Q model, $Q(f) = Q_0 \cdot f^{\eta}$, within 0.3–2.0 Hz, we obtained Q_0 (1 Hz Q) and the frequency-dependence coefficient η of Q for individual geo-blocks (Table S3 in Supporting Information S1).

The Q_{Lg} changes dramatically near the NE boundary of the Tibetan Plateau. To identify regions with sharp Q variations, we calculated the Q gradient of the broadband Q_{Lg} using the central finite-difference method (Text S2 in Supporting Information S1). Based on the high-Q gradient contour (gradient $\ln Q = 6 \times 10^{-3}$ km^{-1}), we can trace a line coinciding with LMSF in the south, heading north along ZLF, and roughly following 39°N in the north to form the boundary (Figure 2f).

Figure 3 compares the broadband (0.3–2.0 Hz) Q_{Lg} and S-velocity distributions. Two low-Q_{Lg} zones were observed, one beneath the Songpan-Ganzi and the West Qinling (LQZ1), and the other beneath the Qilian orogen in the north (LQZ2). They are separated by a high-Q_{Lg} and high-Vs Gonghe Basin (GB) (Figures 3a and 3e). The LQZ1 is limited to the south of 36°N, while LQZ2 is bounded by SQS to the south and NQTF to the north (Figures 3a, 3c, 3d, and 3f). The distribution of low-Q_{Lg} anomalies correlates well with the low S-wave velocities distributed in the middle-lower crust (Han et al., 2022) (Figure 3 and Figure S9 in Supporting Information S1), indicating a widespread weak middle-to-lower crust along the NE margin of the Tibetan Plateau. The Sichuan Basin, Longxi Basin, Ordos, and Alxa are characterized by relatively high Q_{Lg} values, consistent with their rigid properties. Notably, small-scale low-Q_{Lg} anomalies (Figure 3a) in the northern Ordos block and the Yinchuan graben do not correlate with low S-velocities at 30 km depth (Figure 3b), indicating that different mechanisms may dominate attenuation in these regions. For example, thick sedimentary sequences in this region reach 4–6 km (Ren et al., 2024; X. C. Wang, Li, et al., 2017), which may cause significant scattering attenuation. The distinct contrast between the low Q_{Lg} within the plateau and the high Q_{Lg} in adjacent areas aligns well with previous Lg attenuation studies (X. Y. Bao et al., 2011; L. F. Zhao et al., 2013), but the current result features much higher resolution and thus can provide better constraints on regional geodynamics.

4. Discussion

4.1. Potential Ductile Crustal Flow Beneath the Songpan-Ganzi Terrane

Strong seismic attenuation usually reflects weak crust and the presence of multi-scale heterogeneities, cracks, fluid content, temperature anomalies, and partial melting (Amalokwu et al., 2014; Karato & Spetzler, 1990; Kong et al., 2013; Mitchell, 1995; Winkler & Nur, 1982). The LQZ1 is consistent with the widespread low shear-wave velocity (X. W. Bao et al., 2013; C. X. Jiang et al., 2014; H. Li et al., 2014; Y. G. Li et al., 2017; X. C. Wang, Li, et al., 2017; P. P. Zhao et al., 2021), high electric conductivity (Bai et al., 2010; X. B. Wang et al., 2014; W. B. Wei et al., 2001), and high Vp/Vs ratio (1.76–1.85) (Xu et al., 2014) observed in the same area. Vs values below 3.4 km/s are considered a sign of crustal partial melting (Yang et al., 2012). The strong attenuation, together with S-wave velocities lower than 3.4 km/s in the middle-lower crust (Figures 3c–3f), indicates that the crust beneath the Songpan-Ganzi and the West Qinling is mechanically weak, possibly due to partial melting.

Usually, increased fluid content or a 5% melt can reduce the viscosity of crustal materials by an order of magnitude (Rosenberg & Handy, 2005), which provided a basis for the middle-lower crust flow model (Clark & Royden, 2000; Royden et al., 1997). Q_{Lg} cross-sections (Figures 3c–3f) show that the LQZ1 beneath the Songpan-Ganzi and West Qinling is closely related to low-velocity anomalies, significant crust thickening, and increasing surface elevation. This implies that deformation of low-viscosity materials may be the primary mechanism for surface uplift at plateau margins. The Songpan-Ganzi lower crust exhibits stronger anisotropy than the middle crust (Hao et al., 2021), likely indicating horizontal migration of ductile materials driven by differential lateral gravitational forces. GPS observations reveal a highly continuous deformation pattern across the Tibetan Plateau, supporting a model of widespread viscous deformation in the lower crust, which in turn influences upper-crust deformation (M. Wang & Shen, 2020). Petrological and geochemical studies have demonstrated that felsic volcanic rocks erupted 4.7–0.3 Ma in central-northern Tibet were generated by the partial melting of crustal rocks, indicating that crustal melting is crucial in triggering crustal weakening and outward flow (Q. Wang et al., 2016). Therefore, the low-Q_{Lg} anomalies in the Songpan-Ganzi and West Qinling are interpreted as indicators of middle-lower crustal ductile flow driven by partial melting, which plays a key role in controlling crustal deformation in this region.

Regarding the extent of potential crustal flow, Figure 3 shows that the ductile crustal materials, indicated by LQZ1, are widely distributed in Songpan-Ganzi, extending from the KLF northeastward into the West Qinling, bounded by WQF to the north and LMSF to the east, without invading the Qilian or Qinling-Dabie orogens. This distribution aligns with the seismic *Vs* and *Vp*/*Vs* profiles (Ye et al., 2017), anisotropy (Hao et al., 2021), and magnetotelluric observations (Zhan et al., 2014). The ductile crustal materials may respond to lateral pressure gradients and flow toward the plateau edge, until they are blocked by the rigid Sichuan Basin to the east, thereby forming the steep topography of the LMSF.

4.2. Brittle Crustal Shortening Beneath the Qilian Orogen

The Qilian orogen in northern NETP may have distinct dynamics. As one of the youngest expansion boundaries of the Tibetan Plateau (Yuan et al., 2013; D. W. Zheng et al., 2010), it absorbs slow northeastward convergence at ~5.5 mm/yr (Figure S10 in Supporting Information S1, P. Z. Zhang et al., 2004). The average Q of LQZ2 beneath the Qilian orogen is 222, which is less pronounced than that in LQZ1 with average $Q_{\mathrm{Lg}} = 167$ (Table S3 in Supporting Information S1). Two major LQZs are separated by the high-Q_{Lg} rigid Qaidam and Gonghe Basin, with no noticeable low-Q_{Lg} connections. Significant differences were also observed in anisotropy (Wu et al., 2023), shear-wave velocity (C. Zheng et al., 2019), and Poisson's ratio (X. C. Wang, Ding, et al., 2017) between the crusts of the Qilian orogen and Songpan-Ganzi. Therefore, the origin of LQZ2 appears to differ from that of LQZ1 and developed independently.

Tectonic deformation in the Qilian orogen is dominated by lateral shortening and vertical thickening through folding or thrusting, as confirmed by receiver functions and radial anisotropy studies (S. Li et al., 2022; Murodov et al., 2023; Shi et al., 2017). Magnetostratigraphic analysis indicates that the initial uplift of the Qilian orogenic belt began at ~13.5–10.5 Ma (W. T. Wang et al., 2016), significantly younger than the central-northern Tibetan Plateau (~42 Ma; Ou et al., 2017). Most of the crustal shortening in the Qilian orogen occurred in the late Miocene, coinciding with the rapid cooling of a series of thrust faults in northern and eastern Qilian (~10–8 Ma; D. W. Zheng et al., 2006, 2010). Therefore, we interpret the LQZ2 beneath the Qilian as a thermal-related intracrustal response to shortening between the NETP and the NCC (e.g., H. Li et al., 2014). The heat may originate from shear heating and radioactive heating accumulated during crustal thickening (Chen et al., 2019; Molnar et al., 1983). Furthermore, the combination of low relief and low seismicity suggests that the interior of the Qilian orogenic belt is developing plateau-like characteristics (Allen et al., 2017). The Qilian orogenic belt likely represents an earlier stage of plateau evolution (S. Li et al., 2022) and has not yet served as a conduit for the extrusion of middle-lower crustal materials from the Tibetan Plateau.

4.3. Expansion Boundary of the Northeastern Tibetan Plateau

It is widely accepted that the vast Tibetan Plateau has undergone stepwise growth (Tapponnier et al., 2001). Exploring the expansion boundaries of the plateau is crucial for deciphering the crustal deformation mechanisms and tectonic evolution (Shen et al., 2017; Yuan et al., 2013). Distinct from the steep topographic variations in the Longmen Shan and Himalayas, gentle slopes exist between NE Tibet and the NCC (Figure 1). Whether the Longxi Basin and Alxa Block (in southwest NCC) are incorporated into the plateau interior remains debated (e.g., Sun et al., 2021; Yuan et al., 2013). Based on Q_{Lg}-gradient data, we propose a concept of a large-scale boundary zone to enhance our understanding of the expanding frontier of the NETP.

Sharp Q_{Lg} variations often occur near the plateau margin. Based on the high-Q gradient contour (gradient $\ln Q = 6 \times 10^{-3}\ \mathrm{km}^{-1}$), a line with a steep Q_{Lg} gradient can be traced in Figure 2f (dashed magenta line). This line starts at the LMSF, where the maximum Q_{Lg} gradient is observed, then runs northward and partially coincides with the boundaries of several tectonic units (e.g., the Sichuan Basin, the Longxi Basin). Finally, it turns west and lies south of the NQTFs, which are known as the northward growth front of the Tibetan Plateau (D. W. Zheng et al., 2017). This spatial pattern aligns with the Qilian orogen having undergone a relatively brief period of deformation (S. Li et al., 2022). To the northeast, the high Q_{Lg}-gradient line partially intrudes the Alxa block, in agreement with previous observations that the lithosphere structure of the western Alxa has been modified (X. C. Wang, Li, et al., 2017). In the east, distinct from the commonly recognized Liupanshan fault (LPSF) as the plateau boundary (Tian et al., 2021), the high Q_{Lg}-gradient line extends southward along the ZLF. Therefore, it appears that the high-Q_{Lg} rigid Longxi Basin has not yet been subsumed by the plateau, which is broadly consistent with the boundary inferred from radial anisotropy observations (S. Li et al., 2022). The high Q_{Lg}-gradient line

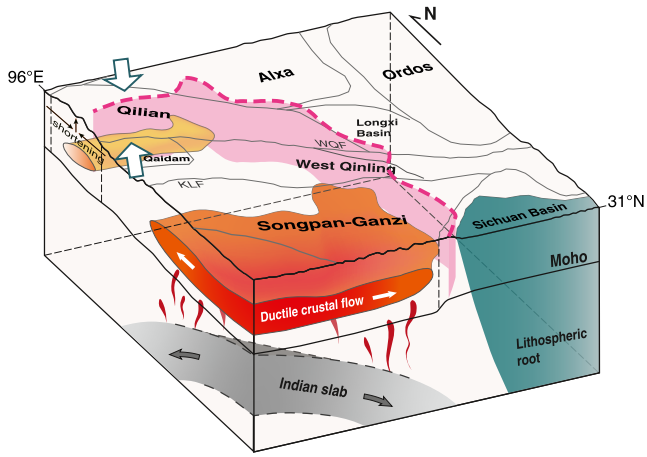

Figure 4. Schematic diagram showing geodynamics beneath the Northeastern (NE) margin of the Tibetan Plateau and possible ductile crustal flow. White arrows within the red middle-lower crust indicate the potential direction of migration. Gray arrows indicate the northeastward subduction of the Indian plate. The green hollow arrows and black arrows, modified from Feng et al. (2020), represent the lateral shortening and uplift of the Qilian orogen, as well as the isolated tectonic response within its crust (yellow patch). The dashed magenta line represents the expansion boundary of the NE Tibetan Plateau derived from the crustal Q_{Lg} gradient.

delineates the strength contrast between the plateau and the foreland, suggesting an expansion boundary of the NETP based on seismic attenuation. Accordingly, our results provide direct constraints on the interpretation of the tectonic framework in the transition zone between the NETP and the foreland (the NCC and Yangtze blocks).

4.4. Tectonic Evolution in NE Tibet Driven by Multiple Dynamics

The crustal deformation in NETP is likely influenced by deep thermal processes, as evidenced by prominent low-velocity zones extending from the middle-lower crust to the upper mantle (Dong et al., 2020; Y. H. Li et al., 2013; Z. G. Wei et al., 2015; C. Zheng et al., 2019). Recent seismic tomographies revealed high-velocity zones at 100–200 km depth, interpreted as the northward-subducting Indian plate (Dong et al., 2020), which has reached or even exceeded the southwestern boundary of the Songpan-Ganzi terrane (Feng et al., 2020; Hou et al., 2024). In this case, the low-Q_{Lg} Songpan-Ganzi may have been affected by mantle thermal upwelling and dehydration associated with the subducting Indian plate. The widespread Cenozoic potassic lavas of mantle origin in western Songpan-Ganzi further support this (Chung et al., 2005). These deep thermal processes likely weakened the lower crust in NE Tibet (Cheng et al., 2016) and, to some extent, facilitated ductile crustal flow (C. S. He et al., 2019; Owens & Zandt, 1997) (Figure 4). This is consistent with the relatively lower heat flow values in NE Tibet (60–70 mW/m^2) (Hu et al., 2000; G. Z. Jiang et al., 2019), since the increase in moisture content would lower the melting point of the crust materials (Molnar et al., 1983). In contrast, the Qilian orogen exhibits low-*Vp*/*Vs* in the crust and uppermost mantle, representing relative coldness and rigidity, which is distinct from the hot and weak pattern (low-*Vs* and high-*Vp*/*Vs*) observed beneath the Songpan-Ganzi (H. L. Li et al., 2022). The Qilian orogen is probably not significantly affected by the deep thermal upwelling.

Based on combined thermochronological and geophysical evidence, it is concluded that the tectonic evolution in NE Tibet conforms to a two-phase mode (E. Wang et al., 2012). The uplift of the Songpan-Ganzi belt occurred concurrently with the India-Eurasia collision (~50 Ma, Clark et al., 2010; Spurlin et al., 2005; Yuan et al., 2013). In the early stage (mid-late Eocene to Miocene), tectonic deformation was primarily characterized by crustal thickening along faults induced by lithospheric compression (E. Wang et al., 2012). Thereafter, the thickened crust underwent thermal weakening, generating partial melting (Beaumont et al., 2004; Nelson et al., 1996). Mantle upwelling, possibly related to the northward subduction of the Indian plate, may accelerate this process, promoting the transition from brittle thickening to ductile crustal flow (Owens & Zandt, 1997). In the later stage (Late Miocene to the present), the mature parts of NE Tibet, such as the Songpan-Ganzi and West Qinling, are dominated by the crustal ductile flow during the geological time scale (E. Wang et al., 2012; Q. Wang et al., 2012; Wu et al., 2023). Ductile crustal flow in NE Tibet may accommodate shallow crustal stress (L. Li et al., 2016) and/or maintain uniform topography through flowing (Owens & Zandt, 1997). The India-Eurasia collisional stress was transmitted northward to the Qilian orogen through the rigid Qaidam Basin (Dupont-Nivet et al., 2002; D. W. Zheng et al., 2010). Starting at ~13.5–10.5 Ma and continuing through the middle to late Miocene, the Qilian orogenic belt underwent rapid uplift (W. T. Wang et al., 2016), representing an early stage of plateau formation (Wu et al., 2023).

5. Conclusion

We constructed a high-resolution broadband crustal *Q* model in NE Tibet using Lg-wave attenuation tomography, incorporating a large, high-quality data set from dense permanent and multi-stage mobile seismic networks, including the ChinArray-Himalaya II. The model reveals a significantly low-Q_{Lg} zone in the Songpan-Ganzi and West Qinling, suggesting that ductile crustal flow is confined south of 36°N without northward extrusion into the Qilian orogen. Moreover, the crust in this region may be affected by deep-mantle upwelling, which promotes the formation of low-viscosity materials within the thickened crust. Another isolated and relatively insignificant low-Q_{Lg} zone beneath the Qilian orogen is likely an intracrustal response to the shortening between the NE Tibet and the NCC, representing an early stage of plateau formation. The high Q_{Lg}-gradient line represents the variations in crustal strength between the plateau and the foreland, indicating an expansion boundary of the NE Tibetan

Plateau. In summary, the ductile crustal flow beneath the Songpan-Ganzi and West Qinling, as well as the vertical thickening that dominates in the Qilian, may have jointly controlled Cenozoic deformation in NE Tibet. These findings extend previous studies and provide new insights into regional geodynamics and their roles in the evolution of NE Tibet.

Conflict of Interest

The authors declare no conflicts of interest relevant to this study.

Data Availability Statement

The waveform data used in this study were collected from the China National Earthquake Data Center, the International Earthquake Science Data Center, and the Incorporated Research Institutions for Seismology Data Management Center (IRIS-DMC). The continuous Lg, pre-event noise, and pre-phase noise waveforms, single- and two-station Lg amplitude data used in this study, and the resulting Lg-wave attenuation model in the NE Tibetan Plateau are available at the World Data Center for Geophysics, Beijing (R. J. Li et al., 2025). Certain figures were generated using Generic Mapping Tools (Wessel & Smith, 1998). Thanks to Shoucheng Han and Haijiang Zhang for providing the USTClitho2.0 seismic velocity model (Han et al., 2022).

Acknowledgments
The comments from Editor F. A. Capitanio, Associate Editor, and two reviewers, A. Mahanama and C. Singh, are valuable and greatly improved this manuscript. This research was supported by the National Natural Science Foundation of China (U2139206).

References

Allen, M. B., Walters, R. J., Song, S. G., Saville, C., De Paola, N., Ford, J., et al. (2017). Partitioning of oblique convergence coupled to the fault locking behavior of fold-and-thrust belts: Evidence from the Qilian Shan, northeastern Tibetan Plateau. *Tectonics*, *36*(9), 1679–1698. https://doi.org/10.1002/2017tc004476

Amalokwu, K., Best, A. I., Sothcott, J., Chapman, M., Minshull, T., & Li, X. Y. (2014). Water saturation effects on elastic wave attenuation in porous rocks with aligned fractures. *Geophysical Journal International*, *197*(2), 943–947. https://doi.org/10.1093/gji/ggu076

Bai, D., Unsworth, M. J., Meju, M. A., Ma, X., Teng, J., Kong, X., et al. (2010). Crustal deformation of the eastern Tibetan plateau revealed by magnetotelluric imaging. *Nature Geoscience*, *3*(5), 358–362. https://doi.org/10.1038/ngeo830

Bao, X. W., Song, X. D., Xu, M. J., Wang, L. S., Sun, X. X., Mi, N., et al. (2013). Crust and upper mantle structure of the North China Craton and the NE Tibetan Plateau and its tectonic implications. *Earth and Planetary Science Letters*, *369*, 129–137. https://doi.org/10.1016/j.epsl.2013.03.015

Bao, X. Y., Sandvol, E., Ni, J., Hearn, T., Chen, Y. S. J., & Shen, Y. (2011). High resolution regional seismic attenuation tomography in eastern Tibetan Plateau and adjacent regions. *Geophysical Research Letters*, *38*(16), L16304. https://doi.org/10.1029/2011gl048012

Beaumont, C., Jamieson, R. A., Nguyen, M. H., & Medvedev, S. (2004). Crustal channel flows: 1. Numerical models with applications to the tectonics of the Himalayan-Tibetan orogen. *Journal of Geophysical Research*, *109*(B6), B06406. https://doi.org/10.1029/2003jb002809

Chen, L., Song, X. D., Gerya, T. V., Xu, T., & Chen, Y. (2019). Crustal melting beneath orogenic plateaus: Insights from 3-D thermo-mechanical modeling. *Tectonophysics*, *761*, 1–15. https://doi.org/10.1016/j.tecto.2019.03.014

Cheng, B., Zhao, D. P., Cheng, S. Y., Ding, Z. T., & Zhang, G. W. (2016). Seismic tomography and anisotropy of the Helan-Liupan tectonic belt: Insight into lower crustal flow and seismotectonics. *Journal of Geophysical Research-Solid Earth*, *121*(4), 2608–2635. https://doi.org/10.1002/2015jb012692

Chung, S. L., Chu, M. F., Zhang, Y. Q., Xie, Y. W., Lo, C. H., Lee, T. Y., et al. (2005). Tibetan tectonic evolution inferred from spatial and temporal variations in post-collisional magmatism. *Earth-Science Reviews*, *68*(3–4), 173–196. https://doi.org/10.1016/j.earscirev.2004.05.001

Clark, M. K., Farley, K. A., Zheng, D. W., Wang, Z. C., & Duvall, A. R. (2010). Early Cenozoic faulting of the northern Tibetan Plateau margin from apatite (U-Th)/He ages. *Earth and Planetary Science Letters*, *296*(1–2), 78–88. https://doi.org/10.1016/j.epsl.2010.04.051

Clark, M. K., & Royden, L. H. (2000). Topographic ooze: Building the eastern margin of Tibet by lower crustal flow. *Geology*, *28*(8), 703–706. https://doi.org/10.1130/0091-7613(2000)028<0703:tobtem>2.3.co;2

Dong, X. P., Yang, D. H., & Zhu, H. J. (2020). Adjoint tomography of the lithospheric structure beneath northeastern Tibet. *Seismological Research Letters*, *91*(6), 3304–3312. https://doi.org/10.1785/0220200135

Dupont-Nivet, G., Butier, R. F., Yin, A., & Chen, X. H. (2002). Paleomagnetism indicates no Neogene rotation of the Qaidam Basin in northern Tibet during Indo-Asian collision. *Geology*, *30*(3), 263–266. https://doi.org/10.1130/0091-7613(2002)030<0263:Pinnro>2.0.Co;2

Efron, B. (1979). Bootstrap methods: Another look at the Jackknife. *Annals of Statistics*, *7*(1), 1–26. https://doi.org/10.1214/aos/1176344552

Feng, M., An, M. J., Mechie, J., Zhao, W. J., Xue, G. Q., & Su, H. P. (2020). Lithospheric structures of and tectonic implications for the central-east Tibetan plateau inferred from joint tomography of receiver functions and surface waves. *Geophysical Journal International*, *223*(3), 1688–1707. https://doi.org/10.1093/gji/ggaa403

Han, S. C., Zhang, H. J., Xin, H. L., Shen, W. S., & Yao, H. J. (2022). USTClitho2.0: Updated unified seismic tomography models for continental China lithosphere from joint inversion of body-wave arrival times and surface-wave dispersion data. *Seismological Research Letters*, *93*(1), 201–215. https://doi.org/10.1785/0220210122

Hao, S. J., Huang, Z. C., Han, C. R., Wang, L. S., Xu, M. J., Mi, N., & Yu, D. Y. (2021). Layered crustal azimuthal anisotropy beneath the northeastern Tibetan Plateau revealed by Rayleigh-wave Eikonal tomography. *Earth and Planetary Science Letters*, *563*, 116891. https://doi.org/10.1016/j.epsl.2021.116891

He, C. S., Dong, S. W., & Wang, Y. H. (2019). Lithospheric delamination and upwelling asthenosphere in the Longmenshan area: Insight from teleseismic P-wave tomography. *Scientific Reports*, *9*(1), 6967. https://doi.org/10.1038/s41598-019-43476-0

He, X., Zhao, L. F., Xie, X. B., Tian, X. B., & Yao, Z. X. (2021). Weak crust in southeast Tibetan Plateau revealed by Lg-wave attenuation tomography: Implications for crustal material escape. *Journal of Geophysical Research-Solid Earth*, *126*(3), e2020JB020748. https://doi.org/10.1029/2020jb020748

Hou, Z. Q., Liu, L. J., Zhang, H. J., Xu, B., Wang, Q. F., Yang, T. N., et al. (2024). Cenozoic eastward growth of the Tibetan Plateau controlled by tearing of the Indian slab. *Nature Geoscience*, *17*(3), 255–263. https://doi.org/10.1038/s41561-024-01382-9

Hu, S. B., He, L. J., & Wang, J. Y. (2000). Heat flow in the continental area of China: A new data set. *Earth and Planetary Science Letters*, *179*(2), 407–419. https://doi.org/10.1016/s0012-821x(00)00126-6

Hubbard, J., & Shaw, J. H. (2009). Uplift of the Longmen Shan and Tibetan plateau, and the 2008 Wenchuan (M=7.9) earthquake. *Nature*, *458*(7235), 194–197. https://doi.org/10.1038/nature07837

Jiang, C. X., Yang, Y. J., & Zheng, Y. (2014). Penetration of mid-crustal low velocity zone across the Kunlun Fault in the NE Tibetan Plateau revealed by ambient noise tomography. *Earth and Planetary Science Letters*, *406*, 81–92. https://doi.org/10.1016/j.epsl.2014.08.040

Jiang, G. Z., Hu, S. B., Shi, Y. Z., Zhang, C., Wang, Z. T., & Hu, D. (2019). Terrestrial heat flow of continental China: Updated dataset and tectonic implications. *Tectonophysics*, *753*, 36–48. https://doi.org/10.1016/j.tecto.2019.01.006

Karato, S., & Spetzler, H. A. (1990). Defect microdynamics in minerals and solid-state mechanisms of seismic wave attenuation and velocity dispersion in the mantle. *Reviews of Geophysics*, *28*(4), 399–421. https://doi.org/10.1029/RG028i004p00399

Karplus, M. S., Klemperer, S. L., Lawrence, J. F., Zhao, W., Mechie, J., Tilmann, F., et al. (2013). Ambient-noise tomography of north Tibet limits geological terrane signature to upper-middle crust. *Geophysical Research Letters*, *40*(5), 808–813. https://doi.org/10.1002/grl.50202

Kong, L. Y., Gurevich, B., Muller, T. M., Wang, Y. B., & Yang, H. Z. (2013). Effect of fracture fill on seismic attenuation and dispersion in fractured porous rocks. *Geophysical Journal International*, *195*(3), 1679–1688. https://doi.org/10.1093/gji/ggt354

Laske, G., Masters, G., Ma, Z., & Pasyanos, M. (2013). Update on CRUST1.0 - A 1-degree global model of Earth's crust. In *Paper presented at the EGU general assembly conference abstracts*.

Li, H., Shen, Y., Huang, Z., Li, X., Gong, M., Shi, D., et al. (2014). The distribution of the mid-to-lower crustal low-velocity zone beneath the northeastern Tibetan Plateau revealed from ambient noise tomography. *Journal of Geophysical Research: Solid Earth*, *119*(3), 1954–1970. https://doi.org/10.1002/2013JB010374

Li, H. L., Ye, Z., Gao, R., & Huang, X. F. (2022). A distinct contrast in the lithospheric structure and limited crustal flow across the northeastern Tibetan Plateau: Evidence from Vs and Vp/Vs imaging. *Tectonophysics*, *836*, 229413. https://doi.org/10.1016/j.tecto.2022.229413

Li, L., Li, A. B., Murphy, M. A., & Fu, Y. Y. V. (2016). Radial anisotropy beneath northeast Tibet, implications for lithosphere deformation at a restraining bend in the Kunlun fault and its vicinity. *Geochemistry, Geophysics, Geosystems*, *17*(9), 3674–3690. https://doi.org/10.1002/2016gc006366

Li, R. J., Zhao, L. F., Xie, X. B., He, X., & Yao, Z. X. (2025). Single- and two-station Lg amplitude data and a broadband Lg attenuation model in and around the northeastern Tibetan Plateau [Dataset]. *World Data Center for Geophysics*. https://doi.org/10.12197/2025GA006

Li, S., Guo, Z., Yu, Y., Wu, X., & Chen, Y. J. (2022). Imaging the northeastern crustal boundary of the Tibetan Plateau with radial anisotropy. *Geophysical Research Letters*, *49*(23), e2022GL100672. https://doi.org/10.1029/2022GL100672

Li, Y. G., Pan, J. T., Wu, Q. J., & Ding, Z. F. (2017). Lithospheric structure beneath the northeastern Tibetan Plateau and the western Sino-Korea Craton revealed by Rayleigh wave tomography. *Geophysical Journal International*, *210*(2), 570–584. https://doi.org/10.1093/gji/ggx181

Li, Y. H., Liu, M. A., Wang, Q. L., & Cui, D. X. (2018). Present-day crustal deformation and strain transfer in northeastern Tibetan Plateau. *Earth and Planetary Science Letters*, *487*, 179–189. https://doi.org/10.1016/j.epsl.2018.01.024

Li, Y. H., Wu, Q. J., Pan, J. T., Zhang, F. X., & Yu, D. X. (2013). An upper-mantle S-wave velocity model for East Asia from Rayleigh wave tomography. *Earth and Planetary Science Letters*, *377*, 367–377. https://doi.org/10.1016/j.epsl.2013.06.033

Mitchell, B. J. (1995). Anelastic structure and evolution of the continental-crust and upper-mantle from seismic surface-wave attenuation. *Reviews of Geophysics*, *33*(4), 441–462. https://doi.org/10.1029/95rg02074

Molnar, P., Chen, W.-P., & Padovani, E. (1983). Calculated temperatures in overthrust terrains and possible combinations of heat sources responsible for the tertiary granites in the greater Himalaya. *Journal of Geophysical Research*, *88*(B8), 6415–6429. https://doi.org/10.1029/JB088iB08p06415

Molnar, P., & Tapponnier, P. (1975). Cenozoic tectonics of Asia: Effects of a continental collision. *Science*, *189*(4201), 419–426. https://doi.org/10.1126/science.189.4201.419

Murodov, D., Zhao, J. M., Wang, X., Murodov, M., Shah, S. T. H., Murodov, A., & Faizulloev, S. (2023). Deep crustal structure across northeastern Tibet from P receiver functions. *Physics of the Earth and Planetary Interiors*, *341*, 107048. https://doi.org/10.1016/j.pepi.2023.107048

Nelson, K. D., Zhao, W., Brown, L. D., Kuo, J., Che, J., Liu, X., et al. (1996). Partially molten middle crust beneath southern Tibet: Synthesis of project INDEPTH results. *Science*, *274*(5293), 1684–1688. https://doi.org/10.1126/science.274.5293.1684

Ou, Q., Wang, Q., Wyman, D. A., Zhang, H.-X., Yang, J.-H., Zeng, J.-P., et al. (2017). Eocene adakitic porphyries in the central-northern Qiangtang Block, central Tibet: Partial melting of thickened lower crust and implications for initial surface uplifting of the plateau. *Journal of Geophysical Research: Solid Earth*, *122*(2), 1025–1053. https://doi.org/10.1002/2016JB013259

Owens, T. J., & Zandt, G. (1997). Implications of crustal property variations for models of Tibetan plateau evolution. *Nature*, *387*(6628), 37–43. https://doi.org/10.1038/387037a0

Paige, C., & Sanders, M. A. (1982). LSQR: An algorithm for sparse linear equation and sparse least squares. *ACM Transactions on Mathematical Software*, *8*, 43–71.

Ren, P., Guo, Z., Liu, Y., Luo, B., & Wu, X. (2024). Seismic evidence of basin development in NE Tibetan Plateau in response to deep crustal dynamics from joint inversion of Rayleigh wave ellipticity and phase velocity. *Geophysical Research Letters*, *51*(18), e2024GL108589. https://doi.org/10.1029/2024GL108589

Rosenberg, C. L., & Handy, M. R. (2005). Experimental deformation of partially melted granite revisited: Implications for the continental crust. *Journal of Metamorphic Geology*, *23*(1), 19–28. https://doi.org/10.1111/j.1525-1314.2005.00555.x

Royden, L. H., Burchfiel, B. C., King, R. W., Wang, E., Chen, Z. L., Shen, F., & Liu, Y. P. (1997). Surface deformation and lower crustal flow in eastern Tibet. *Science*, *276*(5313), 788–790. https://doi.org/10.1126/science.276.5313.788

Shen, X., Liu, M., Gao, Y., Wang, W., Shi, Y., An, M., et al. (2017). Lithospheric structure across the northeastern margin of the Tibetan Plateau: Implications for the plateau's lateral growth. *Earth and Planetary Science Letters*, *459*, 80–92. https://doi.org/10.1016/j.epsl.2016.11.027

Shi, J. Y., Shi, D. N., Shen, Y., Zhao, W. J., Xue, G. Q., Su, H. P., & Song, Y. (2017). Growth of the northeastern margin of the Tibetan Plateau by squeezing up of the crust at the boundaries. *Scientific Reports*, *7*(1), 10591. https://doi.org/10.1038/s41598-017-09640-0

Spurlin, M. S., Yin, A., Horton, B. K., Zhou, J., & Wang, J. (2005). Structural evolution of the Yushu-Nangqian region and its relationship to syncollisional igneous activity east-central Tibet. *Geological Society of America Bulletin*, *117*(9–10), 1293–1317. https://doi.org/10.1130/b25572.1

Sun, Q., Pei, S. P., Cui, Z. X., Chen, Y. J., Liu, Y. B., Xue, X. T., et al. (2021). A new growth model of the northeastern Tibetan Plateau from high-resolution seismic imaging by improved double-difference tomography. *Tectonophysics*, *798*, 228699. https://doi.org/10.1016/j.tecto.2020.228699

Tapponnier, P., Xu, Z. Q., Roger, F., Meyer, B., Arnaud, N., Wittlinger, G., & Yang, J. S. (2001). Oblique stepwise rise and growth of the Tibet plateau. *Science*, *294*(5547), 1671–1677. https://doi.org/10.1126/science.105978

Tian, X. B., Bai, Z. M., Klemperer, S. L., Liang, X. F., Liu, Z., Wang, X., et al. (2021). Crustal-scale wedge tectonics at the narrow boundary between the Tibetan Plateau and Ordos block. *Earth and Planetary Science Letters*, *554*, 116700. https://doi.org/10.1016/j.epsl.2020.116700

Wang, E., Kirby, E., Furlong, K. P., van Soest, M., Xu, G., Shi, X., et al. (2012). Two-phase growth of high topography in eastern Tibet during the Cenozoic. *Nature Geoscience*, *5*(9), 640–645. https://doi.org/10.1038/ngeo1538

Wang, M., & Shen, Z. K. (2020). Present-day crustal deformation of continental China derived from GPS and its tectonic implications. *Journal of Geophysical Research-Solid Earth*, *125*(2), e2019JB018774. https://doi.org/10.1029/2019jb018774

Wang, Q., Chung, S.-L., Li, X.-H., Wyman, D., Li, Z.-X., Sun, W.-D., et al. (2012). Crustal melting and flow beneath northern Tibet: Evidence from Mid-Miocene to Quaternary strongly peraluminous rhyolites in the southern Kunlun range. *Journal of Petrology*, *53*(12), 2523–2566. https://doi.org/10.1093/petrology/egs058

Wang, Q., Hawkesworth, C. J., Wyman, D., Chung, S. L., Wu, F. Y., Li, X. H., et al. (2016). Pliocene-Quaternary crustal melting in central and northern Tibet and insights into crustal flow. *Nature Communications*, *7*(1), 11888. https://doi.org/10.1038/ncomms11888

Wang, W. T., Zhang, P. Z., Pang, J. Z., Garzione, C., Zhang, H. P., Liu, C. C., et al. (2016). The Cenozoic growth of the Qilian Shan in the northeastern Tibetan Plateau: A sedimentary archive from the Jiuxi Basin. *Journal of Geophysical Research-Solid Earth*, *121*(4), 2235–2257. https://doi.org/10.1002/2015jb012689

Wang, X. B., Zhang, G., Fang, H., Luo, W., Zhang, W., Zhong, Q., et al. (2014). Crust and upper mantle resistivity structure at middle section of Longmenshan, eastern Tibetan plateau. *Tectonophysics*, *619*, 143–148. https://doi.org/10.1016/j.tecto.2013.09.011

Wang, X. C., Ding, Z. F., Wu, Y., & Zhu, L. P. (2017). Crustal thicknesses and Poisson's ratios beneath the northern section of the north-south seismic belt and surrounding areas in China (in Chinese). *Chinese Journal of Geophysics-Chinese Edition*, *60*(6), 2080–2090. https://doi.org/10.6038/cjg20170605

Wang, X. C., Li, Y. H., Ding, Z. F., Zhu, L. P., Wang, C. Y., Bao, X. W., & Wu, Y. (2017). Three-dimensional lithospheric S wave velocity model of the NE Tibetan Plateau and western North China Craton. *Journal of Geophysical Research-Solid Earth*, *122*(8), 6703–6720. https://doi.org/10.1002/2017jb014203

Wei, W. B., Unsworth, M., Jones, A., Booker, J., Tan, H. D., Nelson, D., et al. (2001). Detection of widespread fluids in the Tibetan crust by magnetotelluric studies. *Science*, *292*(5517), 716–718. https://doi.org/10.1126/science.1010580

Wei, Z. G., Chen, L., Jiang, M. M., & Ling, Y. (2015). Lithospheric structure beneath the central and western North China Craton and the adjacent Qilian orogenic belt from Rayleigh wave dispersion analysis. *Tectonophysics*, *646*, 130–140. https://doi.org/10.1016/j.tecto.2015.02.008

Wessel, P., & Smith, W. H. F. (1998). New, improved version of generic mapping tools released. *Eos, Transactions American Geophysical Union*, *79*(47), 579. https://doi.org/10.1029/98EO00426

Winkler, K. W., & Nur, A. (1982). Seismic attenuation: Effects of pore fluids and frictional sliding. *Geophysics*, *47*(1), 1–15. https://doi.org/10.1190/1.1441276

Wu, X. Y., Guo, Z., Li, S. L., Yu, Y., Bai, Q. P., & Chen, Y. J. (2023). Seismic azimuthal anisotropy of northeastern Tibetan Plateau from ambient noise double beamforming tomography: Implications for crustal deformation. *Journal of Geophysical Research-Solid Earth*, *128*(6), e2022JB026109. https://doi.org/10.1029/2022jb026109

Xie, J., & Mitchell, B. J. (1990). Attenuation of multiphase surface waves in the basin and range province: Part I. Lg and Lg coda. *Geophysical Journal International*, *102*(1), 121–137. https://doi.org/10.1111/j.1365-246X.1990.tb00535.x

Xu, T., Wu, Z. B., Zhang, Z. J., Tian, X. B., Deng, Y. F., Wu, C. L., & Teng, J. W. (2014). Crustal structure across the Kunlun fault from passive source seismic profiling in East Tibet. *Tectonophysics*, *627*, 98–107. https://doi.org/10.1016/j.tecto.2013.11.010

Yang, Y. J., Ritzwoller, M. H., Zheng, Y., Shen, W., Levshin, A. L., & Xie, Z. (2012). A synoptic view of the distribution and connectivity of the mid-crustal low velocity zone beneath Tibet. *Journal of Geophysical Research*, *117*(B4). https://doi.org/10.1029/2011JB008810

Ye, Z., Gao, R., Li, Q. S., Zhang, H. S., Shen, X. Z., Liu, X. Z., & Gong, C. (2015). Seismic evidence for the North China plate underthrusting beneath northeastern Tibet and its implications for plateau growth. *Earth and Planetary Science Letters*, *426*, 109–117. https://doi.org/10.1016/j.epsl.2015.06.024

Ye, Z., Li, J. T., Gao, R., Song, X. D., Li, Q., Li, Y., et al. (2017). Crustal and uppermost mantle structure across the Tibet-Qinling transition zone in NE Tibet: Implications for material extrusion beneath the Tibetan Plateau. *Geophysical Research Letters*, *44*(20), 10316–10323. https://doi.org/10.1002/2017GL075141

Yuan, D. Y., Ge, W. P., Chen, Z. W., Li, C. Y., Wang, Z. C., Zhang, H. P., et al. (2013). The growth of northeastern Tibet and its relevance to large-scale continental geodynamics: A review of recent studies. *Tectonics*, *32*(5), 1358–1370. https://doi.org/10.1002/tect.20081

Zhan, Y., Zhao, G. Z., Wang, L. F., Wang, J. J., Chen, X. B., Zhao, L. Q., & Xiao, Q. B. (2014). Deep electric structure beneath the intersection area of West Qinling orogenic zone with North-South Seismic tectonic zone in China (in Chinese). *Chinese Journal of Geophysics-Chinese Edition*, *57*(8), 2594–2607. https://doi.org/10.6038/cjg20140819

Zhang, P. Z., Shen, Z., Wang, M., Gan, W. J., Burgmann, R., Molnar, P., et al. (2004). Continuous deformation of the Tibetan Plateau from global positioning system data. *Geology*, *32*(9), 809–812. https://doi.org/10.1130/g20554.1

Zhang, S. Y., Ge, Z. X., & Guo, Z. (2022). Characteristics and removal of continuous topographic scattering in dense array receiver function imaging. *Journal of Geophysical Research-Solid Earth*, *127*(5), e2021JB023683. https://doi.org/10.1029/2021jb023683

Zhao, L. F., Xie, X. B., He, J. K., Tian, X. B., & Yao, Z. X. (2013). Crustal flow pattern beneath the Tibetan Plateau constrained by regional Lg-wave Q tomography. *Earth and Planetary Science Letters*, *383*, 113–122. https://doi.org/10.1016/j.epsl.2013.09.038

Zhao, L. F., Xie, X. B., Wang, W. M., Zhang, J. H., & Yao, Z. X. (2010). Seismic Lg-wave Q tomography in and around Northeast China. *Journal of Geophysical Research*, *115*(B8). https://doi.org/10.1029/2009jb007157

Zhao, P. P., Chen, J. H., Li, Y., Liu, Q. Y., Chen, Y. F., Guo, B. A., & Yin, X. Z. (2021). Growth of the northeastern Tibetan Plateau driven by crustal channel flow: Evidence from high-resolution ambient noise imaging. *Geophysical Research Letters*, *48*(13), e2021GL093387. https://doi.org/10.1029/2021gl093387

Zheng, C., Zhang, R. Q., Wu, Q. J., Li, Y. H., Zhang, F. X., Shi, K. X., & Ding, Z. F. (2019). Variations in crustal and uppermost mantle structures across eastern Tibet and adjacent regions: Implications of crustal flow and asthenospheric upwelling combined for expansions of the Tibetan plateau. *Tectonics*, *38*(8), 3167–3181. https://doi.org/10.1029/2018tc005276

Zheng, D. W., Clark, M. K., Zhang, P. Z., Zheng, W. J., & Farley, K. A. (2010). Erosion, fault initiation and topographic growth of the North Qilian Shan (northern Tibetan Plateau). *Geosphere*, *6*(6), 937–941. https://doi.org/10.1130/ges00523.1

Zheng, D. W., Wang, W., Wan, J., Yuan, D., Liu, C., Zheng, W., et al. (2017). Progressive northward growth of the northern Qilian Shan–Hexi Corridor (northeastern Tibet) during the Cenozoic. *Lithosphere*, *9*(3), 408–416. https://doi.org/10.1130/l587.1

Zheng, D. W., Zhang, P.-Z., Wan, J., Yuan, D., Li, C., Yin, G., et al. (2006). Rapid exhumation at ~8 Ma on the Liupan Shan thrust fault from apatite fission-track thermochronology: Implications for growth of the northeastern Tibetan Plateau margin. *Earth and Planetary Science Letters*, *248*(1), 198–208. https://doi.org/10.1016/j.epsl.2006.05.023

References From the Supporting Information

Brune, J. N. (1970). Tectonic stress and the spectra of seismic shear waves from earthquakes. *Journal of Geophysical Research*, *75*(26), 4997–5009. https://doi.org/10.1029/JB075i026p04997

Herrmann, R. B., & Kijko, A. (1983). Short-period Lg magnitudes: Instrument, attenuation, and source effects. *Bulletin of the Seismological Society of America*, *73*(6A), 1835–1850. https://doi.org/10.1785/bssa07306a1835

Ottemöller, L. (2002). Lg wave Q tomography in Central America. *Geophysical Journal International*, *150*(1), 295–302. https://doi.org/10.1046/j.1365-246X.2002.01715.x

Ottemöller, L., Shapiro, N. M., Singh, S. K., & Pacheco, J. F. (2002). Lateral variation of Lg wave propagation in southern Mexico. *Journal of Geophysical Research*, *107*(B1). https://doi.org/10.1029/2001jb000206

Street, R. L., Herrmann, R. B., & Nuttli, O. W. (1975). Spectral characteristics of the Lg wave generated by central United States earthquakes. *Geophysical Journal of the Royal Astronomical Society*, *41*(1), 51–63. https://doi.org/10.1111/j.1365-246X.1975.tb05484.x